Transactions on Electrical and Electronic Materials (2023) 24:140–148
https://doi.org/10.1007/s42341-023-00429-9

Online ISSN 2092-7592
Print ISSN 1229-7607

REGULAR PAPER

Liquid Phase Exfoliation and Characterization of Few Layer MoS_2 and WS_2 Nanosheets as Channel Material in Field Effect Transistor

Rohit Sharma[1] · Ashish Kumar[2] · Anit Dawar[3] · Sunil Ojha[3] · Ambuj Mishra[3] · Anshu Goyal[4] · Radhapiyari Laishram[4] · V. G. Sathe[5] · Ritu Srivastava[2] · Om Prakash Sinha[1]

Received: 23 September 2022 / Revised: 27 December 2022 / Accepted: 5 January 2023 / Published online: 12 January 2023
© The Korean Institute of Electrical and Electronic Material Engineers 2023

Abstract

Field effect transistors (FETs) are considered as the backbone of electronic industry. In this study, we adopted a simple drop cast method for the fabrication of MoS_2 and WS_2 channel based FET on commercially available pre-patterned OFET devices. The synthesis of few-layers thick MoS_2 and WS_2 nanosheets (NSs) has been done by solvent-assisted exfoliation method. FESEM and TEM study reveals that NSs have lateral dimensions in micron and have polycrystalline nature. From XPS, it is observed that MoS_2 NSs has 2H phase whereas WS_2 have hybrid 1T and 2H phase. The frequency difference in Raman vibrational mode for MoS_2 and WS_2 NSs is 24.08 cm^{-1} and 63.84 cm^{-1} respectively, confirms that number of layers is reduced after sonication. UV–visible spectroscopy reveals that the bandgap is 1.7 eV and 1.8 eV for MoS_2 and WS_2 NSs respectively. Later, these nanosheets have been drop-casted as the channel material on pre-patterned FETs devices and their output and transfer characteristics have been studied. It found that the current On/Off ratio is 10^4 and 10^3 for MoS_2 and WS_2-FET device respectively. This facile fabrication of FET devices may provide a new stage for researchers who do not have access of lithography facilities for FET fabrication.

Keywords MoS_2 & WS_2 nanosheets · Structural and optical properties · Electrical properties · FET device

1 Introduction

Nowadays the electronic industry majorly relies on the field effect transistors (FETs) and thus it is also known as backbone of the industry. FETs have gained tremendous attention over the past decades because they enable the upcoming applications in nano-electronic [1–5]. Conventional semiconductors such as silicon faces the several performance limitations such as miniaturization of channel length which introduce the short channel effect, drain induced barrier limitation (DIBL) etc. [6]. Therefore, search for other material is required. In this process, two dimensional (2D) atomically thin materials offer the superior optical and electronic properties, thermoelectric properties, mechanical properties [7–10] and could be explored for the nano-electronic application. 2D materials have MX_2 i.e. X-M-X (where M is Mo/W-atom & X is S-atom) type structure [2]. The layer of TMDs are held together by weak Vander Waal coupling as well as strong in-plane covalent bonding [11, 12].

Exfoliation of these materials are still challenging for researchers, especially with an atomically thin layers. Several synthesis procedures have been so far developed e.g. mechanical exfoliation, hydrothermal method, chemical vapor deposition (CVD), ion intercalation, and liquid phase exfoliation [13–21]. Out of these methods, mechanical exfoliation results in high quality of TMD materials, but this process could not be used for the industrial scale synthesis and does not allow to control the lateral dimension and thickness of flake [22]. Ion intercalation generally changes the electronic properties of TMDs by changing their structure from 2H polytype to 1T type [19]. Another disadvantage of this method is aggregation of nanosheets after removal of

✉ Om Prakash Sinha
opsinha@amity.edu

1 Amity Institute of Nanotechnology, Amity University Uttar Pradesh, Noida, India

2 CSIR- National Physical Laboratory, New Delhi, India

3 Inter University Accelerator Centre, Aruna Asaf Ali Marg, New Delhi, India

4 Solid State Physics Laboratory, Timarpur, New Delhi, India

5 UGC-DAE Consortium for Scientific Research, University Campus, Khandwa Road, Indore, India

ion, safety issue due to lithium-ion and it is time-consuming process. CVD gives better quality, but not suitable for the device integration due to high temperature synthesis and costly instrument [23, 24]. Out of all these methods, liquid-phase exfoliation is a most promising method as it allows the synthesis of a large area of nanosheets and cost efficient. So far these exfoliated TMDs have been used for the serval applications such as optoelectronic applications, logic devices, energy harvesting, and storage devices [3, 24].

Molybdenum (Mo) and Tungsten (W) sulfides are particularly promising channel material in FETs because of their immunity to short channel effect, high mobility, and high on/off ratio [19, 20]. The earlier reports, on transition dichalcogenides, suggests that these materials could be employed for sensing and energy harvesting devices [25–27]. To date in FETs, contacts on the top of MoS_2 and WS_2 flakes were fabricated by e-beam lithography and photolithography which involves multiple processing steps and leaves the residue on the surface [28–31]. These residues may affect the quality of the channel material and cause alternation in electrical properties [24, 32]. To overcome this problem, several methods have been proposed out of which lithography-free fabrication is the best approach. Dry transferring of 2D materials such as MoS_2, phosphorene, HfS_2 on the location on the pre-patterned substrate to get the desired geometry reported in the literature [33–36]. The fabrication of FET devices is very tedious and not a cost-efficient. It required a lot of effort to setup the fabrication facility which is not accessible for every researcher. Therefore, simple approach is required for the fabrication of FET for those researchers which do not have the sophisticated facilities for the fabrication.

To provide an easy solution of above stated issues, we have synthesized a few-layer of MoS_2 and WS_2 nanosheets (NSs) by the LPE method and characterized by field emission scanning electron microscopy (FESEM), transmission electron microscopy (TEM) with selected area electron diffraction (SAED), High resolution X-ray diffraction (HRXRD), X-ray photoelectron spectroscopy (XPS), Raman spectroscopy, UV–Visible spectroscopy. We have demonstrated a simple approach for the fabrication of multilayer MoS_2 and WS_2 channel-based FET devices on pre-patterned OFET substrate which not only produces the high yield device but also removes the undesirable steps of wet chemistry. This work may provide an alternative option for FET fabrication without having a lithography setup at research labs.

2 Experimental Section

2.1 Synthesis of MoS_2 and WS_2 Nanosheets

MoS_2 and WS_2 bulk powder (Alfa Aesar, 90% < 2 μm), N-methyl-pyrrolidone (NMP) (Sigma Aldrich) has been used for synthesis of 2D-MoS_2/WS_2 nanosheets by liquid phase exfoliation (LPE) route because of their high yield and cost-effectiveness. In this process, we take the 10 mg/ml concentration of bulk powder in NMP in a glass vial. The prepared suspension has been sonicated for 8 h in a bath sonicator. Once the sonication process has been done vials are left overnight and solutions are centrifuge at 3000 rpm for 15 min. The supernatant is collected in the glass vials. The supernatants have been characterized by a different characterization technique. These 2DMs have been drop casted on the organic field effect transistor (OFET) chips (O-FET gen-4 devices, Fraunhofer, Germany). The source/drain are 40 nm thick of gold, separated by the 230 nm thick dielectric layer of silicon dioxide (SiO_2), as shown in Fig. 1a.

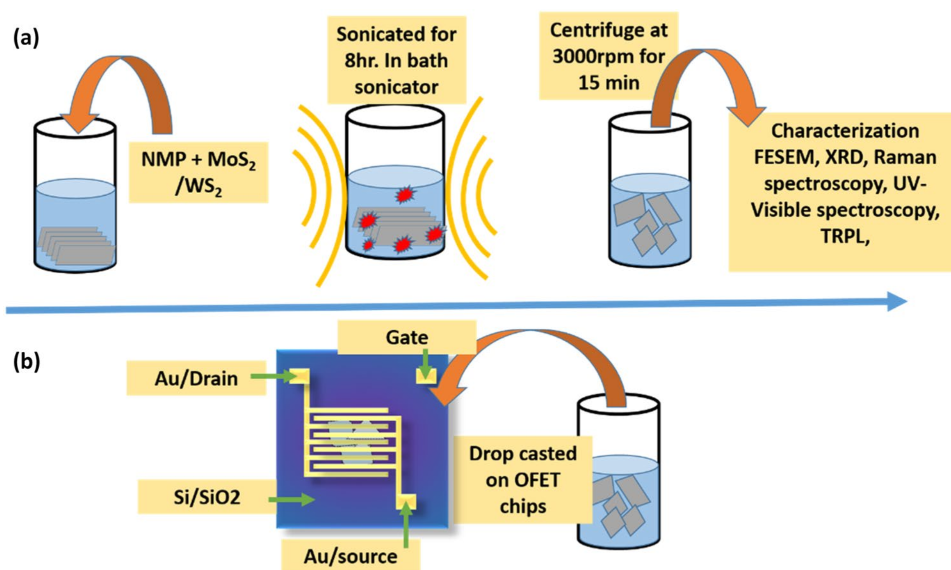

Fig. 1 **a** synthesis procedure of MoS_2 and WS_2 nanosheets **b** fabrication of OFET device

2.2 Characterization Techniques

Structural and morphological study of the prepared samples are analyzed by 200 keV, high-resolution transmission electron microscopy (HRTEM) with selective area electron diffraction (SAED) (JEOL JEM-F200 with Gatan OneView Camera), Field emission electron microscopy (FESEM) (JEOL, JSM-7610F), High resolution X-ray diffractometer (HRXRD) (Bruker D8, 3 kW X-ray generator with Cu target, LynxEye detector, LiF monochromator), Raman spectrometer (Horiba Jobin–Yvon Labram HR) and X-ray photoelectron spectroscopy (XPS) (Omicron Germany EA125 analyzer with 0.6 eV resolution), respectively. The optical properties of prepared sample were studied by the UV–Visible spectrometer (UV-2401PC UV–Visible spectrometer, SHIMADZU). The electrical properties of FET devices have been studied by Keithley (2612A) instrument with a four-probe setup.

3 Result and Discussion

3.1 FESEM and TEM Studies

The samples have been prepared by drop-casting the nanosheets for FESEM and TEM measurements. The surface topography of MoS_2 and WS_2 NSs have been shown in Fig. 2a, b which is recorded by FESEM. Figure 2a, b shows the randomly distributed exfoliated MoS_2 and WS_2 NSs. These exfoliated NSs have been agglomerated due the drop casting method. NSs have lateral dimensions in micron and thickness is upto few layers. In the Fig. 3a, b,

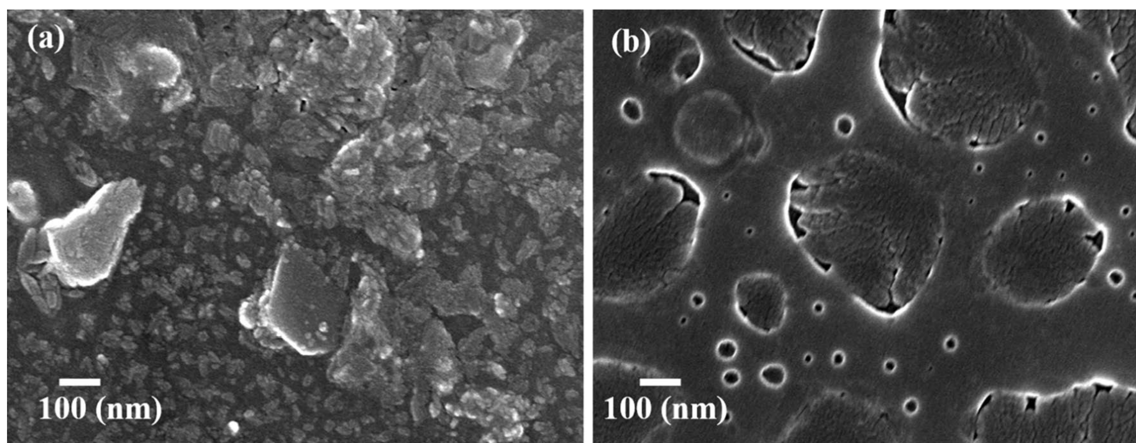

Fig. 2 **a** FESEM image MoS_2 and **b** nanosheets of WS_2 at 100 nm scale

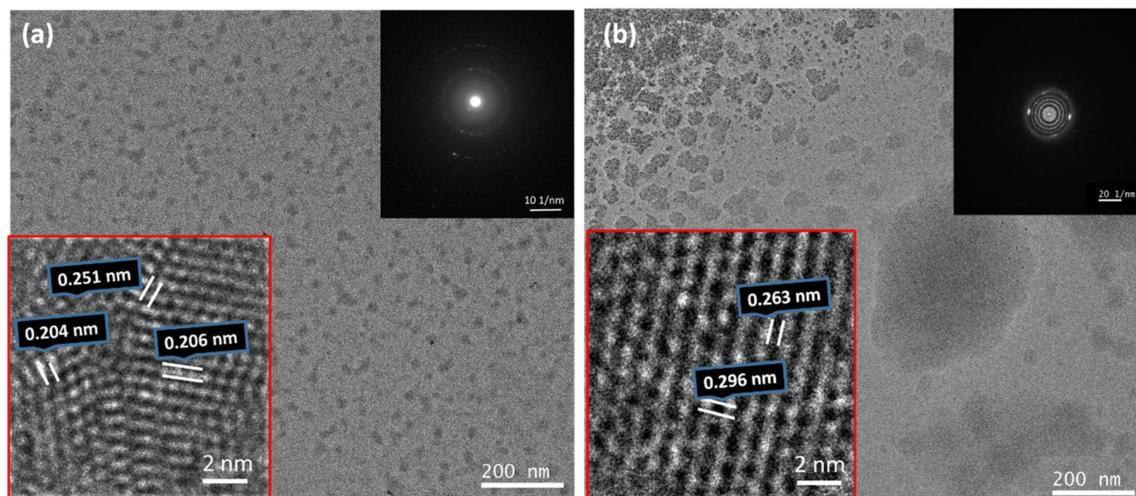

Fig. 3 TEM images of **a** MoS_2 NSs, and **b** WS_2 NSs. The inset images of Fig. 3a show the HRTEM and SAED images. On the other hand, the inset images of Fig. 3b show the HRTEM and FFT images

TEM images show a large number of thin flakes of MoS_2 and WS_2, respectively. The HRTEM images of MoS_2 and WS_2 NSs are shown in inset of Fig. 3a, b with 2 nm scale, respectively. The HRTEM image of MoS_2 nanosheets shows that the regular lattice fringes with an interplanar distance of ~ 0.251, ~ 0.206 and ~ 0.204 nm correspond to the planes (012), (006) and (014), respectively, as indexed in inset of Fig. 3a. Similarly, the HR-TEM image of WS_2 nanosheets, indexed in inset of Fig. 3b, shows the regular lattice fringes with an interplanar distance of ~ 0.263 and ~ 0.296 nm corresponding to the planes (011) and (004) respectively, which belongs to 2H phase of WS_2 [29, 30]. The SAED image, inset of Fig. 3a, and the FFT image, inset of Fig. 3b, confirm the polycrystalline nature of MoS_2 and WS_2 nanosheets, respectively.

3.2 HRXRD Studies

The structural properties of MoS_2 and WS_2 have been studied by X-ray diffraction (XRD) and Raman spectroscopy. XRD patterns of MoS_2 and WS_2 have been shown in Fig. 4 and reveal that NSs have polycrystalline nature. As shown in the figure the peak found for MoS_2 NSs at $2\theta = 14.30°$ belong to (002), plane, (JCPDF-00-037-1492), whereas for WS_2 peak occurred at $2\theta = 14.25°$ represent the (002) miller plane (JCPDF no. 98-001-6261). The peak at 24.31° is of quartz that comes from the substrate. From, XRD pattern it was found that both MoS_2 and WS_2 spectra have a 2H-hexagonal structure with a P3mm/c space group [37]. The reduction in the intensity of (002) plane reveals that the number of the layer in bulk MoS_2 and WS_2 is reduced to few layer [11]. Hence, the structure is stacked along c-axis, and a reduction of particle size is allocated on the (002) plane.

3.3 Raman Spectroscopy

To examine the molecular fingerprint of layered materials Raman spectroscopy is commonly used technique. Raman spectra of MoS_2 and WS_2 are shown in Fig. 5. There are two modes of vibration that occurred in MoS_2 and WS_2: (i) E^1_{2g} which belongs to the in-plane vibration of S-Mo-S atoms in opposite direction and (ii) A_{1g} because of out of plane vibration of S-atom [38] shown in the inset of Fig. 4. As observed, the in-plane mode (E^1_{2g}) for MoS_2 and WS_2 is 383.02 cm^{-1} and 357.12 cm^{-1}, respectively whereas the A_{1g} mode is shifted to 407.60 cm^{-1} and 420.96 cm^{-1} respectively. This blue shift in peaks corresponds to the gain in energy of a scattered photon from the material. The frequency difference (ΔK) between the vibrational mode of bulk MoS_2 and WS_2 is 26.02 cm^{-1} and 70 cm^{-1} [23, 39, 40]. The noticeable ΔK is 24.08 cm^{-1} and 63.84 cm^{-1} for MoS_2 and WS_2 respectively [27, 40, 41]. This also suggested the reduction in thickness of layered material and confirms that the synthesized NSs are few layer thick.

3.4 X-ray Photoemission Spectroscopy (XPS)

The elemental composition and oxidation state of MoS_2 and WS_2 NSs have been recorded by the XPS measurements. The XPS profile after background subtraction and peak smoothing were further processed to closely locate the peaks to identify possible valence state of MoS_2 and WS_2. For Mo-3d orbital, S-2p orbital and W-4f orbital XPS spectra have been shown in Fig. 6a–d having various peaks belongs to singlet of S-2s at 226.1 eV, doublet of Mo^{4+} (3d) at 232.08 eV (Mo^{4+} $3d_{3/2}$), 228.8 eV (Mo^{4+} $3d_{5/2}$), and Mo^{6+} state at 235.2 (Mo^{6+} $3d_{3/2}$) eV, reported [42, 43]. The Mo^{6+}

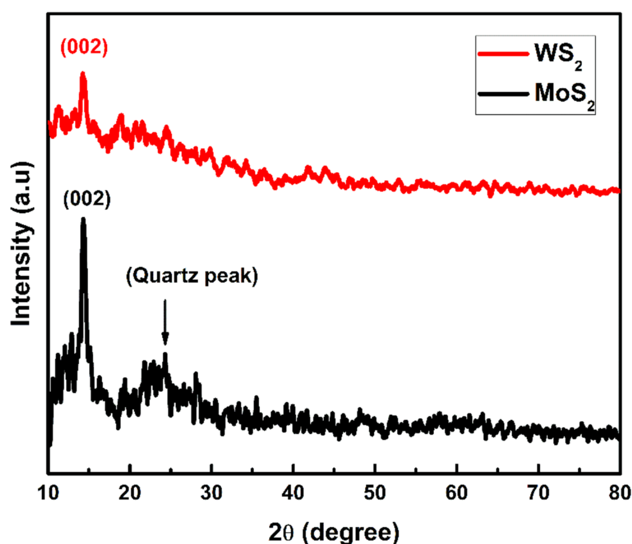

Fig. 4 HRXRD pattern of MoS_2 and WS_2 nanosheets

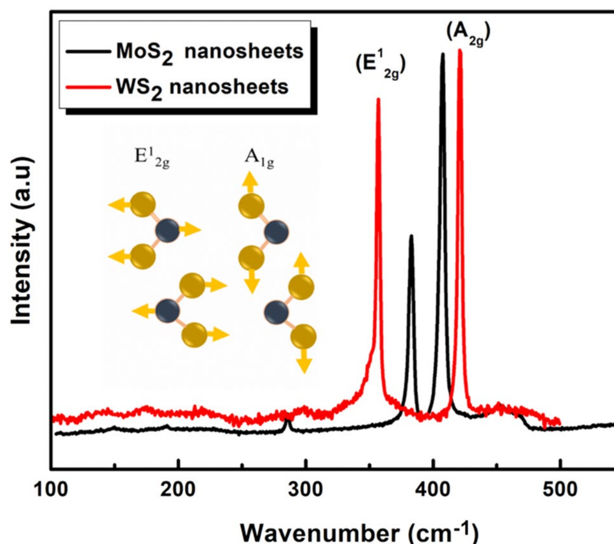

Fig. 5 Raman spectra of MoS_2 and WS_2 nanosheets

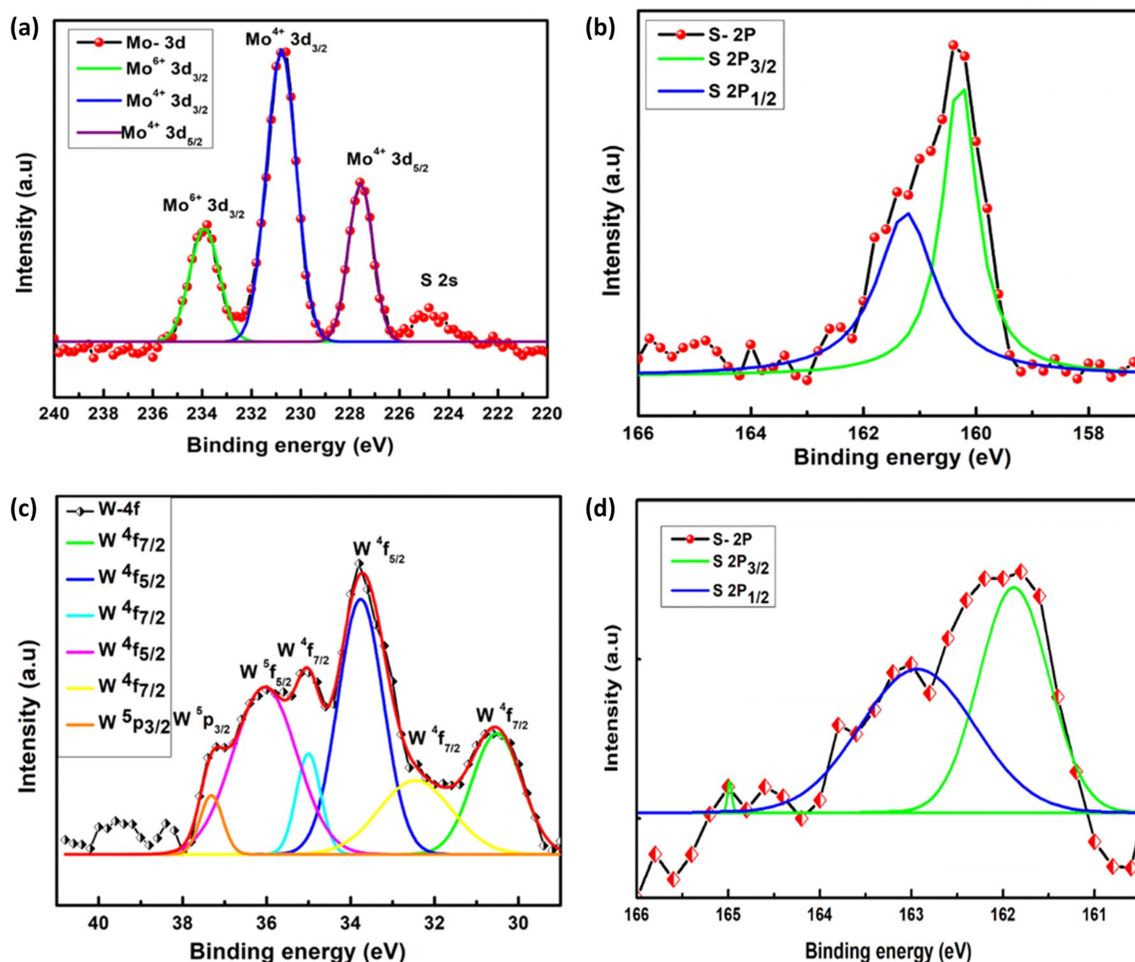

Fig. 6 **a**, **b** XPS spectra of the MoS_2 Mo-3d and S-2p orbital. **c**, **d** XPS spectra WS_2 of W-4f and S-2p orbital

is originated from the partial oxidation of Mo atoms at the edges or the vacant sites of MoS_2 NSs. The S-2p region spectra of MoS_2 are shown in Fig. 6b, which shows the doublet at 160.4 eV and 161.4 eV have been indexed to S $2p_{3/2}$ and S $2p_{1/2}$ [42] which are in good agreement with the binding energy of Mo^{4+} and S^{2-} ion in 2H phase of MoS_2. Due to the atmospheric O_2 on the surface, relative ratio of oxidized Mo^{6+} to Mo^{4+} is increased and which results in the decrease in S/Mo ratio (1:1.45), Also increased in the relative Mo^{6+} means that the edge sites are more chemically active. Thus, larger flakes tend to more oxidized. Finally, the oxidation at the chemically reactive edge site would account for increase in the population of Mo^{6+}.

XPS spectra of core-level of $W4f_{7/2}$, $W4f_{5/2}$ and S-2p have been shown in Fig. 6c, d which is an efficient way to distinguish the metallic 1T' and 2H phase of WS_2. The peaks located at 35 eV and 36 eV ascribed to a doublet of $W4f_{7/2}$ and $W4f_{5/2}$ belongs to 1T metallic phase of WS_2 NSs whereas the two strong peaks at 32.4 eV and 33.8 eV belong to the 2H structure of WS_2 NSs as shown in Fig. 6c. This confirms that the synthesized WS_2 has a mixed phase of 1T and 2H. Meanwhile, the peaks occurred to 37.2 eV and 30.5 eV (W $5p_{3/2}$ and W $4f_{7/2}$) originated from amorphous WOx-clusters on the surface of synthesized WS_2 NSs [44]. Figure 6d shows the deconvulated peaks corresponds to the S $2p_{1/2}$ and s $2p_{3/2}$ at 163.2 eV and 162.1 eV respectively. These value match coherently with the previously reported value for WS_2 nanosheets [41].

3.5 UV–Visible Spectroscopy

The optical properties of MoS_2 and WS_2 have been studied by UV–visible spectrometer. The absorbance spectra and tauc plot of MoS_2 and WS_2 are shown in Fig. 7a, b. In the absorbance spectra of MoS_2 NSs, four excitonic peaks occurred at (a) 668 nm, (b) 610 nm, (c) 446 nm, and (d) 394 nm and excitonic peaks for WS_2 occurs at (1) 634 nm, (2) 526 nm, and (3) 464 nm which match with the literature [20, 45, 46]. The peak (a), (b), and (1) occurred due to the direct excitonic transition at K-point in the Brillouin zone

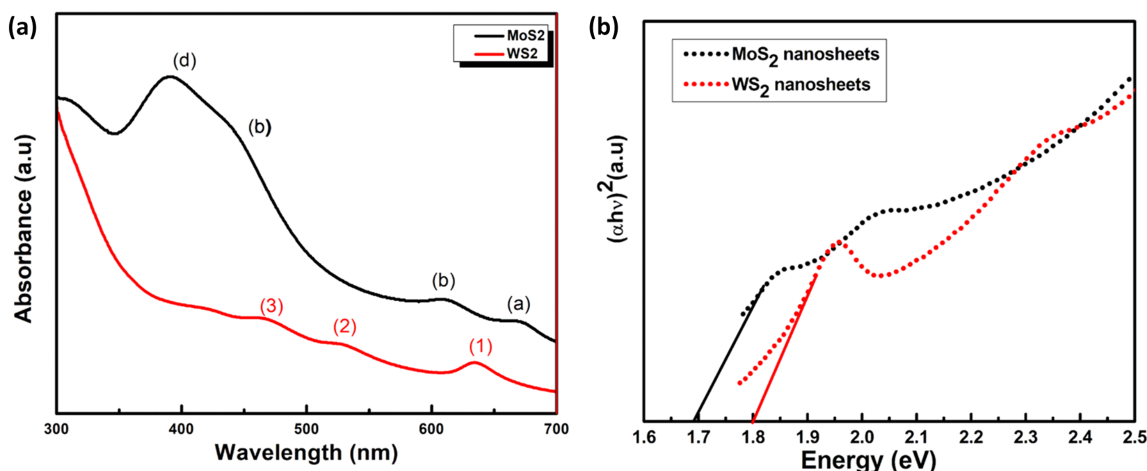

Fig. 7 **a** Absorbance spectra of the MoS_2 and WS_2 nanosheets **b** Tauc plot of MoS_2 and WS_2 nanosheets

and the two peaks appeared due to spin–orbit splitting at K-point [20, 45]. Rest peaks at (c) and (d) for MoS_2 NSs and (2), (3) for WS_2 NSs occurred due to the direct transition at M-point in the Brillouin zone. Also, the von-hove singularity that occurred in crystalline solids at non-smooth points is responsible for these peaks [20]. The optical bandgap of the material is calculated by Tauc equation [47], which is given below:

$$(\alpha h\nu)^{1/n} = A\left(h\nu - E_g\right) \tag{1}$$

$$\alpha = {}^{(2.303 * A)}/_{t} \tag{2}$$

where α, h, A, t, E_g, and ν are the absorption coefficient, Planck's coefficient, optical path length, optical bandgap, and the optical transition frequency, respectively. The value of n can be taken ½ for the direct bandgap. The bandgap of MoS_2 and WS_2 NSs have 1.7 eV and 1.8 eV respectively [35, 45]. The bandgap of MoS_2 and WS_2 is higher than their bulk counterpart which is due to the quantum confinement effect and increases in the surface to volume ratio [39].

3.6 Electrical Properties

The nanosheets have been used as the channel material in commercially precurred pre-patterned FET device (schematic shown Fig. 1b). Figure 8a, b shows the FESEM image of field-effect transistor of MoS_2 and WS_2 (fabrication of devices have been described in the experimental section). The device is annealed at 473 K in a vacuum oven before measurement for the removal of residual contamination. The electrical characterization has been perfromed in an ambient environment using a probe station with Keithley (2612A). The gold electrode on the top acts as drain and source and Si-substrate acts as gate electrode which controls the channel current. The MoS_2 and WS_2 nanosheets assembled on Si/SiO_2 substrate results in conducting channel between 2.5 µm wide gold electrode. Further, the high magnification FESEM image of these devices is shown in Fig. 8a, b. The electrical response of FET deviecs is shown Fig. 8c–f. The linear relationship between I_{ds} and V_{ds} in the plot show good electrical contact between the channel material and Au-contact. Also, there is a clear transition from linear to cut-off region in the output characterstics. The transfer characteristics of MoS_2 and WS_2 channel-based FET devices have been shown in Fig. 8d, f. As, gate voltage could not pass throug the oxide layer, therefore the control performance of devices is not obvious. As observed in FESEM image (Fig. 8a, b), it seems that the channel alignment problem arised from the drop cast method which affects the electrical performance of FET devices due to which the contact resistance is high. The back gate voltage (V_{gs}) is sweeped from V_{gs} 1 V to −5 V at constant $V_d = 0$ V for MoS_2 and for WS_2, $V_{gs} = -6$ V to 6 V at constant $V_d = 0$ V. The on/off ratio and threshold voltage is (V_{th}) of the device is 10^4 and −1.74 V respectively, for MoS_2-FET. The maximum on-state drain current is the order of 10^{-9}A, while the off-state current is 10^{-12}A. The on/off ratio and threshold voltage is (V_{th}) device is 10^3 & −0.47 V for WS_2-FET devices, respectively. The current on/off ratio of the devices is lesser than the reported literature shown in Table 1. The leakage current for both FETs is higher because of different charge state present in MoS_2 and WS_2 which can be visualized from XPS. These valance state act as the charge trap state which contribute to the leakage current. The indirect nature of exciton is consistence and under the biasing, dissociation of exictions occur and generate the 'e' and 'h' [48] and inevitable oxidation states confimed from the XPS could leads to the uneven distribution of potential across the plane of channel materials, which leads to change in the local charge density. This local change in density of charge carrier is reponsible for the drain currrent when $V_d = 0$ V in WS_2-FET. The both

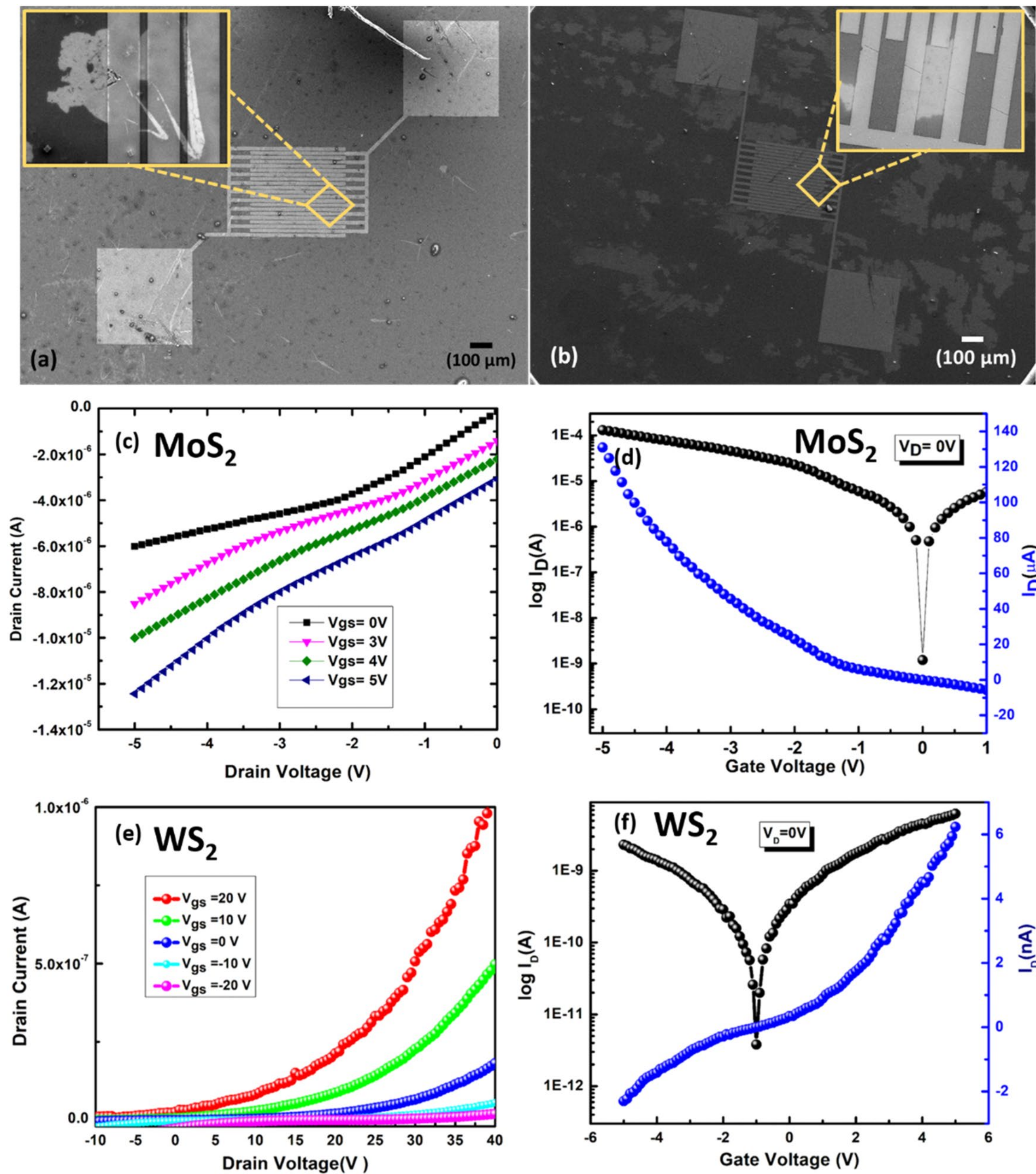

Fig. 8 **a**, **b** FESEM image of MoS_2 and WS_2 nanosheets channel-based FET devices **c**–**f** transfer and output characteristics of MoS_2 and WS_2 nanosheets channel-based FET devices

MoS_2 and WS_2 FETs exhibit bipolar nature, in which hole and electron conduction is shown on the right and left side of the dirac point respectively, in the transfer characterstics of both FETs (Fig. 8d, f) similar behaviour is reported by Fu et al. in 2021 in which they have transfer the graphene over the pattern substrate [49]. Despite, the conductivity is lowest but still it is not zero. The increase current on/off ratio suggest that MoS_2 have better carrier mobility [50] but due to the contribution of several flakes we are not able to predict the current density and mobility of these devices. Also, change in V_{th} is due to the different workfunction of the MoS_2 and $WS_{2.}$ This fabrication method shows a simple approach for the fabrication of MoS_2 and WS_2 device.

4 Conclusion

MoS_2 and WS_2 2DMs as a channel have been actively explored for FET application. MoS_2 and WS_2 NSs have been synthesized via liquid-phase exfoliation method by

Table 1 Comparison from literature

S. No	Materials	Synthesis route and morphology	Current on/off ratio	Threshold voltage (V)	References
1	Graphene	Mechanical exfoliation, NSs	~1.5		Echtermeyer et al. [1]
2	MoS_2	Mechanical exfoliation, Monolayer NS	$\sim 10^6$	–	Kim et al. [51]
3	MoS_2,WSe_2	ALD, NSs	–	−2.7, −3 V respectively	Liang et al. [30]
4	WS_2	Mechanical exfoliation, Monolayer NS	10^6	–	Ovchinnikov et al. [32]
5	WS_2/h-BN	CVD, flake	10^5	–	Han et al. [5]
6	MoS_2	CVD, NSs	10^5	−59.0	Zhang et al. [24]
7	MoS_2 and WS_2	MOCVD, Monolayer	$\sim 10^7$	~2–4 & ~5–8 respectively	Sebastian et al. [21]
8	MoS_2	Mechanical exfoliation, NSs	–	0.9	Zhao et al. [50]
9	MoS_2 and WS_2	LPE, NSs	10^4, 10^3	−1.74, −0.47 respectively	Current work

NSs nanosheets, *LPE* liquid phase exfoliation, *CVD* chemical vapor deposition, *ALD* atomic layer deposition

using NMP as a solvent. Morphological and structural study reveals that the prepared MoS_2 has a few-layer thick 2H semiconducting phase whereas WS_2 has mixed 1T and 2H phases. From Raman spectra, it was found that the frequecny difference between the vibration mode for MoS_2 and WS_2 is 24.08 cm^{-1} and 63.84 cm^{-1} respectively, which confirms the reduction in number of layer of 2D materials. Mo-3d and W-4f doublet peaks have been observed in MoS_2 and WS_2 elemental analysis by XPS. From the optical studies, we have found that the bandgap of MoS_2 and WS_2 NSs is 1.7 eV and 1.8 eV, respectively.These exfoliated NSs have been cast off as the channel material for the OFET chips. The metal-semicondcuctor interface is formed at the contact and have schottky diode like behavior which is shown in the trasfer chacterstics of FET devices and both devices exhabits the bipolarity in nature. The electrical properties reveal that the current on/off ratio for MoS_2 is 10^4 while for WS_2 it is 10^3.

Acknowledgements The authors are thankful to IUAC for extending the FE-SEM facility funded by the Ministry of Earth Sciences (MoES) under the Geochronology project [MoES/P.O.(Seismic)8(09)-Geochron/2012]. We would like to thanks the DRDO-SSPL (Project CAR-1115/CARS-64/TS/SPL/18) for providing financial support for this work.

Data Availability The datasets used and/or analyzed during the current study are available from the corresponding author on reasonable request.

Declarations

Conflict of interest The authors declare that they have no conflict of interest.

References

1. T.J. Echtermeyer, M.C. Lemme, M. Baus, B.N. Szafranek, A.K. Geim, H. Kurz, IEEE Electron Device Lett. **29**, 952 (2008)
2. W. Choi, N. Choudhary, G.H. Han, J. Park, D. Akinwande, Y.H. Lee, Mater. Today **20**, 116–130 (2017)
3. X.R. Wang, Y. Shi, R. Zhang, Chin. Phys. B **22**, 098505 (2013)
4. M. Houssa, A. Dimoulas, A. Molle, *2D Materials for Nanoelectronics* (CRC Press, Boca Raton, 2016)
5. T. Han, H. Liu, S. Chen, S. Wang, K. Yang, Micromachines **12**, 1006 (2021)
6. K. Kuhn, *CMOS and Beyond CMOS: Scaling Challenges* (Elsevier Ltd., Amsterdam, 2018)
7. S. Bertolazzi, J. Brivio, A. Kis, ACS Nano **5**, 9703 (2011)
8. K.F. Mak, C. Lee, J. Hone, J. Shan, T.F. Heinz, Phys. Rev. Lett. **105**, 136805 (2010)
9. R. Bhatt, S. Bhattacharya, R. Basu, M. Patel, A. Singh, P. Bhatt, D.K. Aswal, S.K. Gupta, AIP Conf. Proc. **1536**, 881 (2013)
10. R. Sharma, A. Kumar, R. Kumari, P. Garg, G. Umapathy, R. Laisharm, S. Ojha, R. Srivastava, O.P. Sinha, ChemistrySelect **6**, 11285 (2021)
11. H.S.S. Ramakrishna Matte, A. Gomathi, A.K. Manna, D.J. Late, R. Datta, S.K. Pati, C.N.R. Rao, Angew. Chem. Int. Ed. **49**, 4059 (2010)
12. A. Kumar, R. Sharma, S. Yadav, S.K. Swami, R. Kumari, V.N. Singh, S. Ojha, J.J. Schneider, R. Srivastava, O.P. Sinha, Dalton Trans. **50**, 3894 (2021)
13. H. Lin, X. Chen, H. Li, M. Yang, Y. Qi, Mater. Lett. **64**, 1748 (2010)
14. J.G. Song, J. Park, W. Lee, T. Choi, H. Jung, C.W. Lee, S.H. Hwang, J.M. Myoung, J.H. Jung, S.H. Kim, C. Lansalot-Matras, H. Kim, ACS Nano **7**, 11333 (2013)
15. S. Das, M. Kim, J.W. Lee, W. Choi, Crit. Rev. Solid State Mater. Sci. **39**, 231 (2014)
16. W. Zhao, R.M. Ribeiro, M. Toh, A. Carvalho, C. Kloc, C. Neto, G. Eda, Appl. Mater. Today **1**, 60 (2015)
17. J.L. Sina Najmaei, Z. Liu, W. Zhou, X. Zou, G. Shi, S. Lei, B.I. Yakobson, J.-C. Idrobo, P.M. Ajayan, Chem. Mater. Mater. **26**, 6371 (2014)
18. G. Liu, H. Ma, I. Teixeira, Z. Sun, Q. Xia, X. Hong, S.C.E. Tsang, Chem. Eur. J. **22**, 2910 (2016)
19. X. Fan, P. Xu, D. Zhou, Y. Sun, Y.C. Li, A.M. Nguyen, M. Terrones, T.E. Mallouk, Nano Lett. **15**, 5956 (2015)
20. V. Forsberg, R. Zhang, J. Bäckström, C. Dahlström, B. Andres, M. Norgren, M. Andersson, M. Hummelgård, H. Olin, PLoS ONE **11**, e0154522 (2016)
21. A. Sebastian, R. Pendurthi, T.H. Choudhury, J.M. Redwing, S. Das, Nat. Commun. **12**, 1 (2021)
22. D. Jariwala, V.K. Sangwan, L.J. Lauhon, T.J. Marks, M.C. Hersam, ACS Nano **8**, 1102 (2014)
23. Y. Zhang, Y. Zhang, Q. Ji, J. Ju, H. Yuan, J. Shi, T. Gao, D. Ma, M. Liu, Y. Chen, X. Song, H.Y. Hwang, Y. Cui, Z. Liu, ACS Nano **7**, 8963 (2013)

24. W. Zhang, J.K. Huang, C.H. Chen, Y.H. Chang, Y.J. Cheng, L.J. Li, Adv. Mater. **25**, 3456 (2013)
25. S. Kim, A. Konar, W. Hwang, J.H. Lee, J. Lee, J. Yang, C. Jung, H. Kim, J. Yoo, J. Choi, Y.W. Jin, S.Y. Lee, D. Jena, W. Choi, K. Kim, Nat. Commun. **3**, 1 (2012)
26. J.S. Kim, H.W. Yoo, H.O. Choi, H.T. Jung, Nano Lett. **14**, 5941 (2014)
27. Z. Jia, J. Xiang, F. Wen, R. Yang, C. Hao, Z. Liu, ACS Appl. Mater. Interfaces **8**, 4781 (2016)
28. J. Zhao, H. Yu, W. Chen, R. Yang, J. Zhu, M. Liao, D. Shi, G. Zhang, ACS Appl. Mater. Interfaces **8**, 16546 (2016)
29. D. Ovchinnikov, A. Allain, Y. Huang, D. Dumcenco, ACS Nano **8**, 8174 (2014)
30. J. Liang, K. Xu, B. Toncini, B. Bersch, B. Jariwala, Y.C. Lin, J. Robinson, S.K. Fullerton-Shirey, Adv. Mater. Interfaces **6**, 1801321 (2019)
31. G. Woo, H.U. Kim, H. Yoo, T. Kim, Nanotechnology **32**, 045702 (2021)
32. X. Tong, E. Ashalley, F. Lin, H. Li, Z.M. Wang, Nano-Micro Lett. **7**, 203 (2015)
33. H. Yang, S. Cai, Y. Zhang, D. Wu, X. Fang, J. Phys. Chem. Lett. **12**, 2705 (2021)
34. H. Kaur, S. Yadav, A.K. Srivastava, N. Singh, J.J. Schneider, O.P. Sinha, V.V. Agrawal, R. Srivastava, Sci. Rep. **6**, 34095 (2016)
35. H. Kaur, S. Yadav, A.K. Srivastava, N. Singh, S. Rath, J.J. Schneider, O.P. Sinha, R. Srivastava, Nano Res. **11**, 343 (2018)
36. H. Kaur, V.V. Agrawal, R. Srivastava, ArXiv Preprint ArXiv arXiv:1701.02476 (2017)
37. S.S. Chou, M. De, J. Kim, S. Byun, C. Dykstra, J. Yu, J. Huang, V.P. Dravid, J. Am. Chem. Soc. **135**, 4584 (2013)
38. H. Li, Q. Zhang, C.C.R. Yap, B.K. Tay, T.H.T. Edwin, A. Olivier, D. Baillargeat, Adv. Funct. Mater. **22**, 1385 (2012)
39. R. Ahmad, R. Srivastava, S. Yadav, D. Singh, G. Gupta, S. Chand, S. Sapra, J. Phys. Chem. Lett. **8**, 1729 (2017)
40. S. Najmaei, Z. Liu, P.M. Ajayan, J. Lou, Appl. Phys. Lett. **100**, 013106 (2012)
41. R. Jha, P.K. Guha, J. Mater. Sci. **52**, 7256 (2017)
42. H.W. Wang, P. Skeldon, G.E. Thompson, Surf. Coat. Technol. **91**, 200 (1997)
43. A.T. Massey, R. Gusain, S. Kumari, O.P. Khatri, Ind. Eng. Chem. Res. **55**, 7124 (2016)
44. Z. Wang, P. Liu, Y. Ito, S. Ning, Y. Tan, T. Fujita, A. Hirata, M. Chen, Sci. Rep. **6**, 2 (2016)
45. A. Splendiani, L. Sun, Y. Zhang, T. Li, J. Kim, C.Y. Chim, G. Galli, F. Wang, Nano Lett. **10**, 1271 (2010)
46. S. Sharma, S. Bhagat, J. Singh, M. Ahmad, S. Sharma, J. Mater. Sci. Mater. Electron. **29**, 20064 (2018)
47. N. Saha, A. Sarkar, A.B. Ghosh, A.K. Dutta, G.R. Bhadu, P. Paul, B. Adhikary, RSC Adv. **5**, 88848 (2015)
48. T. Mueller, E. Malic, Npj 2D Mater. Appl. **2**, 1 (2018)
49. Y. Fu, Z. Li, Q. Wang, Phys. Lett. A **391**, 127139 (2021)
50. X.Y. Zhao, L. Liu, J.P. Xu, IEEE Trans. Electron Devices **68**, 3087 (2021)
51. H.C. Kim, H. Kim, J.U. Lee, H.B. Lee, D.H. Choi, J.H. Lee, W.H. Lee, S.H. Jhang, B.H. Park, H. Cheong, S.W. Lee, H.J. Chung, ACS Nano **9**, 6854 (2015)

Publisher's Note Springer Nature remains neutral with regard to jurisdictional claims in published maps and institutional affiliations.

Springer Nature or its licensor (e.g. a society or other partner) holds exclusive rights to this article under a publishing agreement with the author(s) or other rightsholder(s); author self-archiving of the accepted manuscript version of this article is solely governed by the terms of such publishing agreement and applicable law.